Food Hydrocolloids 159 (2025) 110615

Contents lists available at ScienceDirect

Food Hydrocolloids

journal homepage: www.elsevier.com/locate/foodhyd

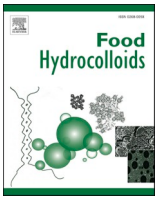

Unravelling the dominant role of phosphorylation degree in governing the functionality of reassembled casein micelles: Implications for future dairy production through precision fermentation

Jing Che [a,*,1], Zekun Fan [b,1], Etske Bijl [b], Julia Prangchat Stub Thomsen [a], Ivan Mijakovic [c,d], Kasper Hettinga [b], Nina Aagaard Poulsen [a], Lotte Bach Larsen [a]

[a] Department of Food Science, Aarhus University, Agro Food Park 48, DK-8200, Aarhus N, Denmark
[b] Food Quality and Design Group, Wageningen University & Research, Bornse Weilanden 9, 6708WG, Wageningen, Netherlands
[c] Systems and Synthetic Biology Division, Department of Biology and Biological Engineering, Chalmers University of Technology, 41296, Chalmers, Sweden
[d] The Novo Nordisk Foundation Center for Biosustainability, Technical University of Denmark, Lyngby, Denmark

ARTICLE INFO

Keywords:
Dephosphorylation
Reassembled casein micelles
Calcium-binding ability
Acid-induced gelation
TEM

ABSTRACT

This study investigated the effect of bovine casein (CN) phosphorylation degree on micelle reassembly, stability, calcium-binding, and acid-induced gelation or precipitation, with the aim of assessing the feasibility of utilising microbial CNs in future dairy production. The four CNs (α_{S1}-, α_{S2}-, β-, and κ-CN) were purified from bovine milk and subjected to enzymatic dephosphorylation, resulting in three pools – fully and partially phosphorylated and fully dephosphorylated. Nine reassembled CN micelle solutions (RCMS) were investigated, consisting of three systems (two of four-CN, and one of β/κ-CN) and three phosphorylation degrees of the corresponding CNs. The distribution of different components (protein, calcium, and phosphorus) into micellar, serum, and insoluble fractions after two centrifugation steps was studied. The pH stability relative to acid-gelation or precipitation of the formed RCMS was further investigated. Results showed that the micelle reassembly ability of RCMS containing all four CNs was proportional to the phosphorylation degree; CNs with higher phosphorylation degrees contained a higher proportion of micelles and exhibited greater calcium-binding ability, whereas fully dephosphorylated CNs hardly formed CN micelle structures. The gelation pH of RCMS increased with decreasing phosphorylation degree, whereas the fully dephosphorylated CNs completely failed in gelation but precipitated when reaching their isoelectric point at pH 5.5. Moreover, RCMS containing only β/κ-CN at their native full phosphorylation were unstable at the salt concentrations applied, with more than half of the CNs self-associating to flocculate. Our study confirms the essential role of phosphorylation degree in micelle reassembly and stability, providing important information for potential future applications of microbial CNs that are expected to exhibit non-native phosphorylation levels.

1. Introduction

Bovine milk plays a fundamental role in human nutrition, with its proteins being widely consumed not only as dairy products but also as functional ingredients in a wide range of foods. However, bovine milk production has been criticised for its negative environmental impacts (Tubiello et al., 2013). Aiming for more climate-friendly milk production, various strategies are being explored, including animal-free production of milk constituents. A key criterion for these milk substitutes to mimic bovine milk functionality is having similar microstructures to milk, essentially casein (CN) micelle structure. CNs, making up 80% of proteins, assemble with salts (mainly calcium and phosphate) and water into micelles in bovine milk (De Kruif & Holt, 2003). These micelles are crucial in dairy production, particularly in processes like milk coagulation and gelation, which are fundamental to yoghurt and cheese manufacturing (Dalgleish & Corredig, 2012; Wang & Zhao, 2022). Therefore, assembling CN micelles that resemble those in milk is a critical step towards the production of animal-free dairy products. It is known that the formation of CN micelles is significantly influenced by post-translational modifications (PTMs), especially phosphorylation,

* Corresponding author.
E-mail address: jing@food.au.dk (J. Che).
[1] First authors: Jing Che and Zekun Fan.

https://doi.org/10.1016/j.foodhyd.2024.110615
Received 5 July 2024; Received in revised form 23 August 2024; Accepted 5 September 2024
Available online 6 September 2024

which is pivotal for preventing calcification in the mammary gland (Bijl et al., 2020; Holt, 1992). Therefore, phosphorylation is indispensable for preserving the nutritional and functional properties of animal-free dairy products.

Among these animal-free strategies, microbial-produced CNs through precision fermentation may offer a viable option for securing the nutritional profile of milk substitutes (Hettinga & Bijl, 2022). Although microbial CNs exhibit amino acid sequences similar to those of bovine CNs, their PTMs may vary - the phosphorylation level of microbial CNs from precision fermentation has been reported to be much lower compared with that of bovine CNs (Hansson et al., 1993; Hettinga et al., 2022). Therefore, to understand the micelle assembly of microbial CNs, it is critical to study the effect of phosphorylation degree on CN micelle formation.

To mimic CN micelle formation and better understand the role of phosphorylation, assembling micelles *in vitro* using dephosphorylated (DP) sodium caseinate (NaCN) or purified CNs together with salts has proved to be a useful approach (Schmidt et al., 1977). This type of CN micelles is called artificial CN micelles (Antuma et al., 2023; Schmidt et al., 1977) or reassembled CN micelles (RCM) (Fan et al., 2024). Earlier studies using this approach demonstrated the importance of phosphorylation in micelle assembly (Antuma et al., 2023; Schmidt & Poll, 1989). However, the effect of lowering the degree of phosphorylation on micelle reassembly and calcium-binding ability has not been extensively studied. In addition, RCM solutions (RCMS) formed using DP CNs showed potential post-production stability issues, with precipitation observed after preparation or during subsequent storage (Schmidt et al., 1989). Therefore, a comprehensive investigation of the different fractions (insoluble, micellar, and serum) of RCMS reassembled by CNs with various degrees of phosphorylation is necessary.

This study aimed to investigate the effect of phosphorylation degree of purified bovine CNs on micelle reassembly, solution stability, calcium-binding ability, and acid-induced gelation or precipitation properties for the evaluation of microbial CNs as future dairy proteins. This was carried out using native fully phosphorylated (FP), partially phosphorylated (PP), and fully DP CNs in three different systems, comprising i) NaCN, ii) purified α_{S1}+α_{S2}/β/κ-CN (αβκ), and iii) purified β/κ-CN (βκ). Two centrifugation steps were applied to separate the insoluble (mild centrifugation), and micellar and serum fractions (ultracentrifugation). The distributions of CNs, calcium, and phosphorus in the obtained fractions at varying degrees of phosphorylation were analysed to assess the compositional aspects of the RCMS and provide insights into the differences in micelle reassembly abilities. Moreover, pH stability relative to acid-gelation or precipitation behaviours of the RCMS was investigated. The knowledge obtained from this study provides a better understanding of the impact of the degree of CN phosphorylation on micelle assembly and functionality, paving the way for the future use of microbial CNs as dairy protein substitutes.

2. Material and methods

2.1. Extraction of CNs

As a model for microbial-produced CNs, bovine CN fractions were isolated from milk using the method described by Sheng et al. (2022), resulting in pools of purified α-CN (α_{S1}+α_{S2}-CN), β-CN, and β+κ-CN. Briefly, 500 mL of unpasteurised bovine skim milk was obtained from the Arla Innovation Centre (Arla Foods, Aarhus N, Denmark) and transferred on ice to the Department of Food Science, Aarhus University. Microbial growth was prevented by adding 0.02% sodium azide. Following the isoelectric precipitation of CNs using 10% CH_3COOH and 1 M CH_3COONa at pH 4.6, the obtained CN precipitate was washed twice with ultrapure water (MilliQ system, Merck KGaA, Darmstadt, Germany). Subsequently, the precipitate was resuspended in 500 mL of ultrapure water with the pH adjusted to 7.0–7.5 and then extensively dialysed against buffer A (20 mM bis-tris propane, 3.3 M urea, 1 mM 1, 4-dithioerythritol, pH 7.0 by HCl) using a dialysis tube with a molecular weight cut-off of 6–8 kDa (Millipore, MA, USA).

Purified α-, β-, and β+κ-CN fractions were obtained by anion exchange fast protein liquid chromatography (FPLC) using GE ÄKTA FPLC™ preparative ion exchange chromatography equipped with UNICORN™ operating system (GE Healthcare/Cytiva) (Sheng et al., 2022). Elution fractions (14 mL) were collected using a Frag-900 fraction collector (GE Healthcare) and monitored under UV light at 214 nm. The purity of each fraction was analysed by SDS-PAGE under reducing conditions, and the fractions were subsequently pooled according to the SDS-PAGE profiles and dialysed against ultrapure water. The resulting α-, β-, and β+κ-CN fractions were further ultra-filtrated to 100 mL and washed five times with ultrapure water (refilled to 400 mL and ultra-filtrated to 100 mL) using Millipore Amicon stirred cells equipped with Ultracel membranes (5 kDa molecular weight cut-off) to remove residual salts, followed by freeze-drying, weighing, and storage at −20 °C until further use.

2.2. Proteomic profiling

The protein contents in the purified CNs as well as in the further RCMS fractions after mild centrifugation and ultracentrifugation (conditions described in *Section 2.6*) were determined by the Dumas combustion method (DUMAS, Rapid N exceed®, Elementar Analysensysteme GmbH, Langenselbold, Germany) using a protein conversion factor of 6.38.

The proteomic profiles of the CNs and RCMS fractions were analysed by a reverse-phase LC-ESI/MS Single Q system equipped with a Jupiter C4 column (250 × 2 mm, 5 μm particle size, 300 Å pore size; Phenomenex), as described earlier (Poulsen et al., 2016; Sheng et al., 2022). Using ChemStation software (Rev.C.01.10, Agilent Technologies), the deconvoluted average masses were matched against an in-house milk protein database to identify the protein isoforms. The relative quantification of specific CNs to the total protein was calculated based on the integration of the specific peak area of the UV signals at 214 nm to the total peak area. As a result, purified α-CN consisted of 75.1% α_{S1}-CN and 18.2% α_{S2}-CN; β-CN had a purity of 89.9%; β+κ-CN was composed of 59.2% β-CN and 38.1% κ-CN (Table S1).

2.3. Enzymatic dephosphorylation of CNs

Dephosphorylation using bovine alkaline phosphatase (BAP, from bovine intestinal mucosa, ≥10 DEA units/mg, Sigma-Aldrich) was conducted according to the method described by Li-Chan and Nakai (1989), with modifications. Briefly, dephosphorylation was performed by dissolving purified CNs in 50 mM Tris-HCl buffers, followed by mixing with an equal volume of the same buffer containing BAP at a protein-to-enzyme ratio of 20 (w/w) for 30 s. Varying phosphorylation degrees were obtained by incubating for different durations at 37 °C. To terminate the reaction, the solution was heated at 80 °C for 10 min.

For CN micelle reassembly, FP, PP (i.e., partially dephosphorylated), and DP CNs were prepared. Specifically, PP NaCN and α-CN were obtained by incubating for 10 min following the addition of BAP, while their DP forms were obtained after 5 h of incubation, both at pH 8.5. For both β-CN and β+κ-CN, incubations of 2 min and 3 h were used to obtain their PP and DP forms, respectively, at pH 7.0. To control for temperature effects, the FP CNs were also heated at 80 °C for 10 min without BAP addition.

2.4. Characterization of phosphorylation degree

Phosphorylation profiles of the samples were further characterised using a reverse-phase LC-ESI/MS Single Q system as described in *Section 2.2*. The area under curve (AUC) of the total ion current (TIC) chromatograms with deconvoluted masses was obtained using Agilent MassHunter BioConfirm software (version 10.0). The major

phosphorylation degree of each CN was calculated based on the ratio of the largest AUC of individual phosphorylation degree relative to total phosphorylation degrees.

2.5. CN micelle reassembly

To explore the potential of using microbial CNs in future dairy manufacturing, three RCMS systems modelled with bovine CNs were prepared. Commercial bovine NaCN (90.1% protein; Sigma-Aldrich) was used to form a standard RCMS system to validate our micelle reassembly method. Additionally, αβκ and βκ systems, reassembled from purified CNs, were employed as models for microbial CNs to assess their functional properties. The three formed RCMS systems with different compositions are shown in Table 1. The CN composition of each system was calculated as the corresponding relative peak area at 214 nm by analysing the whole RCMS using a reverse-phase LC-ESI/MS Single Q system.

Specific amounts of the relevant materials were calculated based on both purity and composition and then weighed to contain a total of 188.5 mg of pure CNs with the corresponding composition. For dephosphorylation, NaCN, purified β-CN, and β+κ-CN were dissolved in 50 mM Tris-HCl buffer at pH 7.0, whereas purified α-CN was dissolved in the same buffer at pH 8.5. In total 188.5 mg of CNs was prepared and dissolved in 2.9 mL of 50 mM Tris-HCl buffer to obtain the final RCMS with 2.6% (w/v) CNs in 20 mM Tris-HCl buffer. Treatments to achieve three degrees of phosphorylation, including FP, PP, and DP CNs, were applied prior to making RCMS.

CN micelles were assembled according to previous studies (Fan et al., 2024; Schmidt et al., 1977) with the following modifications. The CN micelles were reassembled by mixing CN solutions with calcium and phosphate salt under controlled conditions using syringe pumps (NE-300, USA) and SI Analytics Titrator (TitroLine® 7000 Automatic titrator, Germany) for 1 h. The final volume of each RCMS was 7.25 mL, and the concentration of the CN and salt was calculated to be 2.6%, 29.6 mM of $CaCl_2$, 4 mM of $MgCl_2$, 12.1 mM of KH_2PO_4, and 12.1 mM of Na_2HPO_4. Micelle assembly was performed at pH 6.7 at room temperature.

2.6. RCMS fractionation

After micelle reassembly, two centrifugation steps were applied to achieve better separation of the micelles from the insoluble fraction. Specifically, mild centrifugation (4000×*g*, 20 min, 22 °C) was performed to remove the insoluble materials. Subsequently, the mildly centrifuged supernatant was subjected to ultracentrifugation (150,000×*g*, 1 h, 22 °C) to separate micelles and serum.

The obtained RCMS fractions, including whole RCMS, mildly centrifuged supernatant, and ultracentrifuged serum, were analysed. The value of insoluble fraction was calculated as the difference between the whole solution and the mildly centrifuged supernatant. Similarly, the value of micellar fraction was calculated as the difference between the mildly centrifuged supernatant and the ultracentrifuged serum.

Table 1
Relative protein composition as determined by LC-ESI/MS of RCMS representing FP[a], PP[b], and DP[c] of three different systems (NaCN[d], αβκ[e], and βκ[f]) before centrifugation.

RCMS	α-CN (%)	β-CN (%)	κ-CN (%)
NaCN-FP NaCN-PP NaCN-DP	43.8 ± 0.0	45.7 ± 0.0	10.4 ± 0.0
αβκ-FP αβκ-PP αβκ-DP	42.2 ± 0.1	47.7 ± 0.1	10.1 ± 0.1
βκ-FP βκ-PP βκ-DP	4.8 ± 0.2	84.1 ± 0.1	11.1 ± 0.1

[a] FP: the caseins were fully phosphorylated in their native form before micelle reassembly.
[b] PP: the caseins were partially dephosphorylated before micelle reassembly.
[c] DP: the caseins were fully dephosphorylated before micelle reassembly.
[d] NaCN: micelles were reassembled using sodium caseinate, comprising α_{S1}-, α_{S2}-, β-, and κ-CNs.
[e] αβκ: micelles were reassembled using a mixture of purified α_{S1}-, α_{S2}-, β-, and κ-CNs.
[f] βκ: micelles were reassembled using a mixture of purified β- and κ-CNs.

2.7. Zeta potential and hydrodynamic diameter (d_H)

Electrophoretic light scattering (ELS) and dynamic light scattering (DLS) were employed to measure the zeta potential of the whole sample and to determine the apparent d_H of the mildly centrifuged supernatant from the RCMS, respectively, using a Malvern Zetasizer Ultra (Malvern Panalytical Ltd., Worcestershire, UK). The samples were diluted 20- or 50-fold (to have an attenuator in the range of 5–8) with ultrapure water (refractive index: 1.33; viscosity: 0.8872 mPa s) immediately before the measurement and were analysed in a DTS1070 capillary cell at 25 °C with backscattering. Measurements were performed in triplicate for each sample. The recorded zeta potential and Z-average d_H were provided by the ZS Xplorer software (version 2.3.1.4).

2.8. Protein and ion distribution analyses

The protein contents of the different fractions (whole solution, supernatant of mild centrifugation, and serum of ultracentrifugation) after RCMS reassembly were determined using DUMAS, as described in *Section 2.2*. The ion concentrations in these fractions were determined using a previously described method (Fan et al., 2024). The total concentrations of calcium, magnesium, phosphorus, sodium, and potassium (Ca^{2+}, Mg^{2+}, P^{5+}, Na^{+}, and K^{+}) were measured using Inductively Coupled Plasma Optical Emission Spectroscopy (ICP-OES) with an Avio 500 ICP-OES system (PerkinElmer, USA). The inorganic anions citrate, phosphate, and chloride ($C_6H_5O_7^{3-}$, PO_4^{3-}, and Cl^{-}) were analysed using ion chromatography (IC; IonPac AS19 column, 4 × 250 mm, Dionex; Thermo Scientific, Sunnyvale). The protein and ion distributions of each fraction were calculated by dividing the value of that fraction by the value of corresponding whole solution.

2.9. Transmission electron microscope (TEM)

Visualisation of the RCM was conducted using negative-stain TEM operating at the Centre for Cellular Imaging at the University of Gothenburg, part of the National Microscopy Infrastructure. Sample preparation for TEM was adapted from Booth et al. (2011) with modifications. In brief, the mildly centrifuged RCMS supernatants were diluted 1:40 with 20 mM Tris-HCl buffer (pH 6.7), and 5 μL were loaded to glow-discharged, carbon-coated copper grids, 300 mesh (Electron Microscopy Sciences, Hatfield, PA, USA, #CF-300Cu). The sample was blotted off after 1 min before being washed twice with 25 μL ultrapure water and stained with 25 μL uranyl formate 0.75% (pH 4.0) for 30 s. The grids containing the samples were imaged using Talos L120C (Thermo Fisher Scientific, Waltham, MA, USA) at 120 kV. Images were acquired at focus using a 4k × 4k BM-Ceta CMOS camera (Thermo Fisher Scientific, Waltham, MA, USA) at a nominal magnification of 8,500x (1.65 nm/pixel).

The average diameter of the CN micelles in each RCMS was calculated using ImageJ software (http://rsb.info.nih.gov/ij/) by manually selecting 200 individual spherical particles.

2.10. Evolution of storage modulus as a function of phosphorylation degree during acidification

A rheometer (MCR 302, Anton Paar, Graz, Austria) was used for the rheological measurements using a concentric cylinder system (CC10/Ti). Samples (1.3 mL of whole RCMS) were mixed with glucono-δ-lactone (GDL; Merck, Darmstadt, Germany) to a final content of 3.0% (w/v) to decrease the pH in a controlled manner to 4.6 within 60 min. Upon GDL addition, the solution was shaken gently for 30 s before being transferred (1.0 mL) to the rheometer. To monitor the gelation process, a strain of 1%, frequency of 1 Hz, and constant temperature of 30 °C were applied. Measurements were taken every 10 s for 1 h. Meanwhile, the pH of the remaining 0.3 mL solution was continuously measured by a pH meter for 1 h, and recorded every 5 min. The gelation or precipitation time was defined as the point when the storage modulus (G') exceeded 1 Pa. The corresponding pH at this point, defined as gelation or precipitation pH, was calculated based on the logarithmic relationship between pH and time ($R^2 > 0.99$).

2.11. Data analysis

Descriptive statistics were computed using Microsoft Excel (Microsoft, Redmond, WA, USA). Results are presented as the mean ± standard deviation of duplicate samples. Data visualisation and ANOVA analysis were performed using OriginPro version 2023b (OriginLab Corp., Northampton, MA, USA). Significant differences for multiple comparisons were determined by one-way or two-way ANOVA with Tukey's test ($p < 0.05$) as indicated in the figure legends. For two-way ANOVA, factor A was RCMS system and factor B was phosphorylation degree. Asterisks indicate levels of statistical significance: $p < 0.05$ (*), $p < 0.01$ (**), $p < 0.001$ (***), $p < 0.0001$ (****). In the figures, data points that do not share a same letter indicate significant differences ($p < 0.05$).

3. Results and discussion

3.1. Determination of phosphorylation degrees after enzymatic dephosphorylations

As shown in Table S1, the protein contents of the purified α-, β-, and β+κ-CN were in the range of 85–88%, with the specified CN constituting at least 90% of the total protein. The initial degree of phosphorylation of purified native CNs was determined using LC-ESI/MS analysis (Fig. 1). The results showed that the purified α_{S1}-CN was mainly of variant B with eight phosphate groups (8P); α_{S2}-CN was mainly of variant A with 12 and 11P; β-CN was mainly of variant A2 with 5P; κ-CN was mainly of variant B with 1P.

Subsequently, enzymatic dephosphorylation of the purified α- and β-CN was performed with BAP incubation. As shown in Fig. 2a, by 0.2 h of incubation at pH 8.5, PP α-CN was obtained with α_{S1}-CN having 3P as the major peak, though also containing 1–5P, and α_{S2}-CN mainly being present in its 4P and 5P forms. Similarly, PP β-CN was obtained after incubation with BAP for 30 s of mixing time at pH 7.0, with 2P being the major peak apart from the 0–3P identified (Fig. 2a'). Furthermore, TIC chromatograms of α-CN at 5 h and β-CN at 3 h confirmed almost complete dephosphorylation (Fig. 2b and b'), with major peaks of 0P and some minor 1–2P peaks remaining for α_{S2}-CN.

Regarding κ-CN, it is well-known that its main form is with 1P (confirmed in Fig. 1b, inset figure), having no calcium-binding ability, and functions mainly as a hairy surface layer of the CN micelle (Dalgleish et al., 2012). Accordingly, the effect of dephosphorylation of κ-CN was not included in the study.

3.2. Confirmation of phosphorylation degree in RCMS and its effect on zeta potential

RCM formations were induced using FP, PP, and DP CNs with

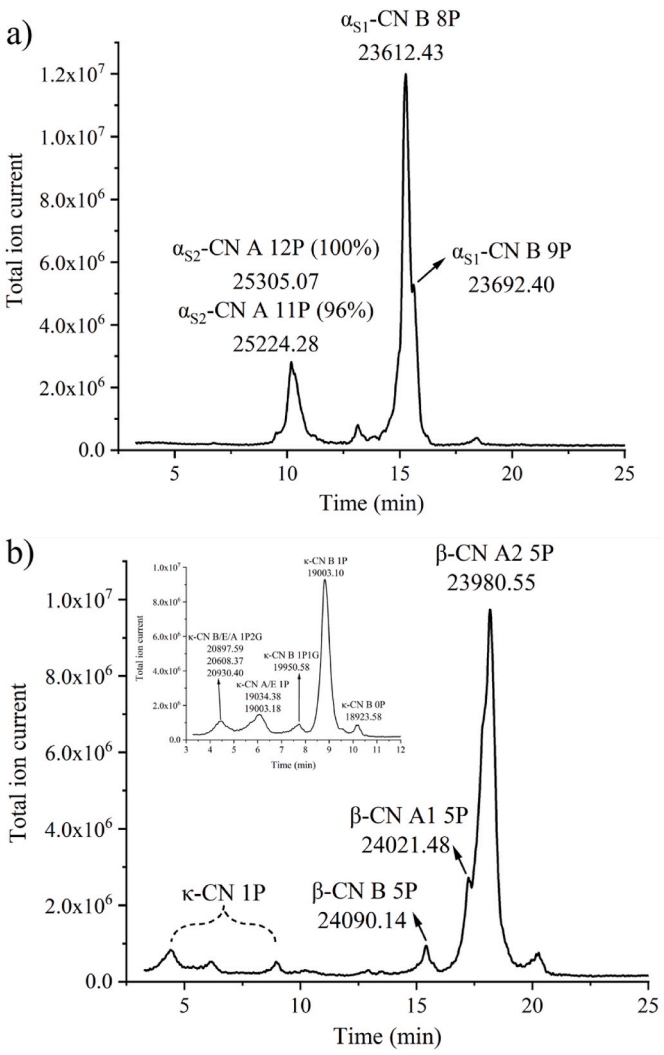

Fig. 1. TIC chromatograms with the deconvoluted masses of purified native fully phosphorylated (FP) **a)** α-CN and **b)** β-CN and κ-CN (inset figure), assessed by LC-ESI/MS single Q analyses and monitored by UV peak area at 214 nm.

progressive addition of calcium and phosphate salts. The degrees of phosphorylation of the CNs in RCMS were assessed using LC-ESI/MS (data not shown). The major phosphorylation profile of the RCMS of NaCN-FP was determined as α_{S1}-CN 75.9% 8P (among 7–9P identified, variant B), α_{S2}-CN 65.6% 12P (11–12P, variant A), β-CN 94.2% 5P (4–5P, mainly variant A2), and 90.5% κ-CN 1P (1–2P, mainly variant A). NaCN-PP was determined as α_{S1}-CN 38.5% 3P (2–6P), α_{S2}-CN 39.8% 4P (4–11P), β-CN 36.8% 1P (0–2P), and 86.3% κ-CN 0P (0–1P). NaCN-DP was determined as α_{S1}-CN 65.8% 1P (0–2P), α_{S2}-CN 56.6% 1P (1, 8, 9P), β-CN 93.7% 0P (0–1P), and κ-CN 100% 0P. These results corresponded with those of the purified CNs.

Zeta potential is an indicator of the surface charge of colloidal particles (Patel et al., 2018), which is often related to the stability of colloidal systems. Zeta potential measurements of the RCMS (Fig. 3) showed that the zeta potential significantly increased with a decreasing degree of phosphorylation in all systems, reflecting decreased electrostatic repulsion between adjacent charged particles by dephosphorylation, suggesting that the stability of RCMS might be affected by the degree of phosphorylation. To further study this, we investigated the distribution of protein, calcium, and salts after two different centrifugation steps, involving first mild centrifugation to remove precipitates, followed by ultracentrifugation of the soluble phase to separate RCM and serum.

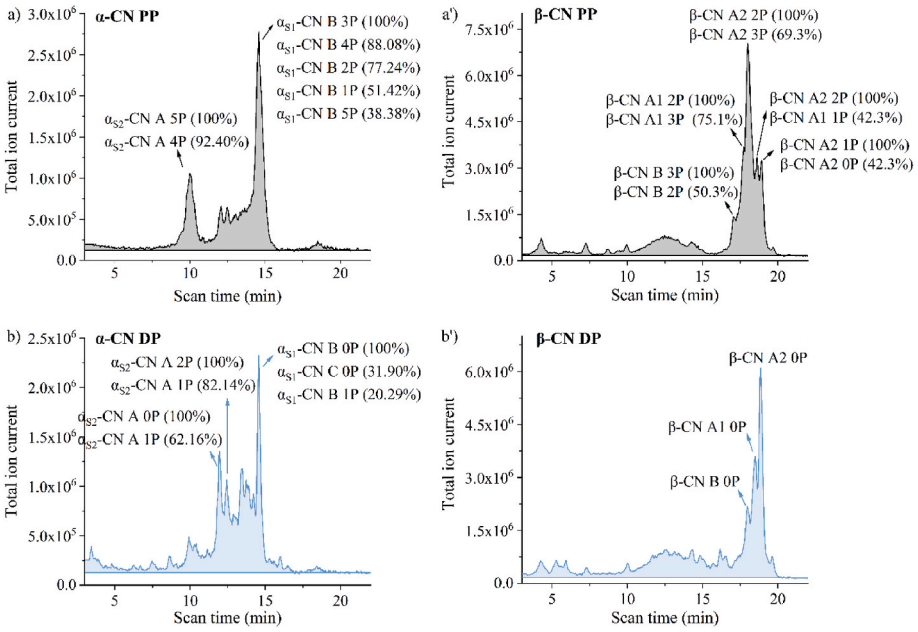

Fig. 2. TIC chromatograms of **a)** α-CN and **a')** β-CN at partially phosphorylated (PP) degree, and **b)** α-CN and **b')** β-CN at fully dephosphorylated (DP) degree, respectively, assessed by LC-ESI/MS single Q analyses and monitored by UV peak area at 214 nm.

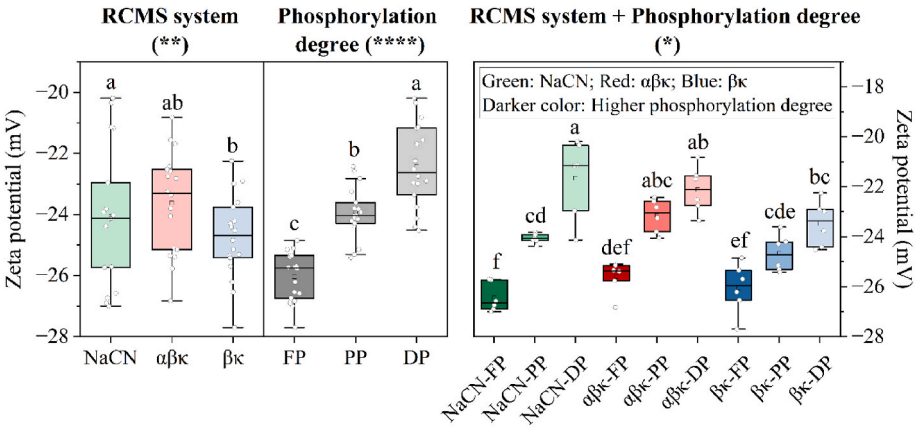

Fig. 3. Zeta potential of the reassembled casein micelle solutions (RCMS) for sodium caseinate (NaCN), α/β/κ-CN (αβκ), and β/κ-CN (βκ) systems at FP, PP, and DP degrees: comparisons across the three RCMS systems ($p = 0.002$, $n = 18$), the three phosphorylation degrees ($p < 0.0001$, $n = 18$), and the interaction effects of RCMS system and phosphorylation degree on zeta potential ($p = 0.038$, $n = 6$). Statistical analysis was performed using two-way ANOVA with Tukey's test.

3.3. *Effect of phosphorylation degree on the stability of RCMS*

Although the structure of CN micelles has not yet been fully elucidated, based on existing research and model discussions, widely acknowledged models involve protein-protein interactions, such as hydrophobic interaction, as well as the bridging of CN and colloidal calcium phosphate (CCP) nanoclusters (CN-CaP interaction) (De Kruif et al., 2012; Horne, 2020). In CN micelles, CCP was sequestered by CN, preventing its growth and forming a stable system together (Holt et al., 2013). Therefore, similar to native CN micelles, the stability of the RCMS is determined by the stability of both CNs and CCP in the micellar fraction. Specifically, CNs should remain stable without precipitating; meanwhile, they should sequester CaP, preventing it from precipitating.

Additionally, in our preliminary experiment, the formation of precipitates in the DP RCMS was observed a few hours after preparation. The composition of these precipitates remained unclear, as literature (Antuma et al., 2023; Fan et al., 2024; Schmidt et al., 1977) typically applied only one centrifugation speed (above 100,000×*g*), resulting in the co-precipitation of the insoluble materials and stable micelles. Therefore, compositional analysis of the precipitates is vital for better understanding their formation mechanism, which could then serve as an indicator of RCMS stability and provide novel insights into the modulation of the assembly process.

Therefore, to investigate RCMS stability, protein and ion distributions among the serum, insoluble, and micellar fractions were analysed, as shown in Fig. 4. The total protein contents of all the RCMS were 2.7 ± 0.1%, and the total concentrations of Ca^{2+} and P^{5+} were 32.2 ± 2.5 mM and 30.1 ± 1.4 mM, respectively.

3.3.1. *Protein contents and distribution in centrifugal fractions of RCMS*

The protein content and composition of the serum, insoluble, and micellar fractions were determined using DUMAS and are shown in Fig. 4a. In the FP RCMS of all three systems, ~87% of the total proteins were sedimentable (sum of insoluble and micellar proteins) by sequential use of the two centrifugation speeds. This is consistent with previous studies where only ultracentrifugation was performed (Antuma et al., 2023; Fan et al., 2024; Schmidt et al., 1977). However, the protein distributions of insoluble and micellar fractions in the sedimentable

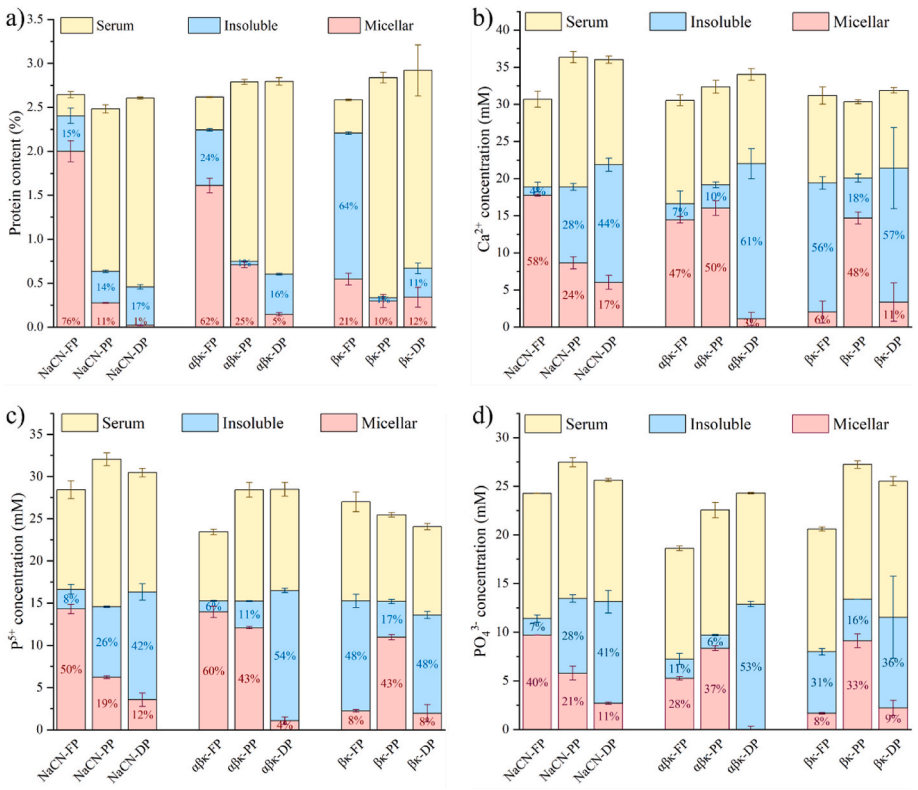

Fig. 4. Protein and salt concentrations and distributions of the indicated RCMS into serum, insoluble, and micellar fractions: **a)** protein content, **b)** Ca^{2+} concentration, **c)** P^{5+} concentration, and **d)** PO_4^{3-} concentration.

phase differed between the four-CN and βκ systems.

It is noted that, for FP RCMS of the four-CN systems (both NaCN and αβκ systems), ~67% of total proteins were in the micellar fraction, with ~20% being insoluble and ~12% being in the serum. However, in both PP and DP RCMS, the protein contents in the micellar fraction decreased notably (to ~18% and ~3%, respectively), while the majority of proteins shifted to the serum fraction (~75 and ~81%, respectively). The protein content and proportion of insoluble proteins did not change considerably with dephosphorylation. These results indicate changes in the distribution of proteins in PP and DP RCMS.

In contrast, the βκ-FP RCMS were found to represent a more unstable system at the employed conditions, with only ~21% of the total protein being micellar while ~64% insoluble apart from ~15% in serum. One explanation for this may be that the lower phosphorylation level of β-CN (mainly 5P) compared with α_{S1}-CN (mainly 8P) and α_{S2}-CN (11–12P) may contribute to the RCMS of only β/κ-CN being less stable, suggested by the similar share of the protein contents of αβκ-PP (possessing mainly 3–5P) and βκ-FP accumulating in the micellar fraction. Interestingly, in βκ-PP and βκ-DP RCMS, the serum protein content increased considerably to ~83%, while much less insoluble protein (~6% of total protein) was formed compared to the βκ-FP. This suggests that the dephosphorylation process improves the CN solubility of βκ RCMS and prevents the CNs from precipitating in the applied system. The possible mechanisms that explain these observations are discussed in *Section 3.3.3*.

3.3.2. *Calcium phosphate (CaP) distribution and within-micelle interactions of four-CN systems*

To investigate the effect of phosphorylation degree on CaP stability, the distributions of Ca^{2+}, P^{5+}, and PO_4^{3-} were studied. As shown in Fig. 4b and c, in all nine RCMS with varying degrees of phosphorylation, ~61% of Ca^{2+} and ~51% of P^{5+} were sedimentable, which is in accordance with previous studies on both RCMS and natural milk (Antuma et al., 2023; Bijl et al., 2013; Fan et al., 2024; Schmidt et al., 1977). However, CaP distribution and stability differed among the FP, PP, and DP RCMS.

For the FP RCMS of the four-CN systems, ~54% and ~45% of the total Ca^{2+} and P^{5+} were in the micellar fraction, respectively, whereas the insoluble fraction accounted for only a minor proportion of ~6% for both Ca^{2+} and P^{5+}. However, in the DP RCMS, micellar Ca^{2+} and P^{5+} (~10% and ~8%, respectively) were markedly lower than those for FP and PP RCMS, whereas considerably increased levels of insoluble Ca^{2+} and P^{5+} were observed (~53% and ~46%, respectively). These results indicate that in the DP RCMS of the four-CN systems, CaP is more prone to be allocated to the insoluble fraction by mild centrifugation than FP or PP. This confirmed a reduced CN-CaP interaction for micelle formation with a decreasing degree of phosphorylation.

Taken together, it can be concluded that in RCMS consisting of the four CNs, as expected, the removal of phosphate groups from the CNs reduces their ability to stabilise CaP and form micelles, leading to easier precipitation of CaP, while the majority of CNs accumulate in the ultracentrifuged serum.

3.3.3. *Calcium phosphate (CaP) distribution and within-micelle interactions of βκ system*

As shown in Fig. 4b and c, in the RCMS of the βκ-FP, the levels of insoluble Ca^{2+} and P^{5+} (~56% and 45%, respectively) were much higher than those observed in the four-CN systems with FP (~6%), and ~7% of both Ca^{2+} and P^{5+} were in the micellar fraction. As described in *Section 3.3.1*, a large portion of CN (~64%) was insoluble, indicating instability of the entire system of βκ-FP. However, the precise reason for this instability remains to be further explored.

Interestingly, when the salt concentration continued to increase during micelle reassembly, the solution was stable for approximately the first half hour (with ~15 mM of Ca^{2+} and PO_4^{3-}) and subsequently formed large chunky flocs during the continuous addition of the salt solutions. This phenomenon suggested that the unstable behaviour of the βκ-FP system may correlate with its lower calcium sequestration capacity (Bijl et al., 2019), likely due to the lower phosphorylation

degree of β-CN compared with α-CNs. In βκ-FP RCMS, the self-associated β/κ-CN (through hydrophobic interaction) are diffused under the long-range electrostatic repulsion from negatively charged phosphate and carboxyl groups. With the progressive addition of Ca^{2+} and PO_4^{3-}, this negative charge is gradually neutralised by binding CaP through phosphoserine residues of β-CN. Micelle structures are formed under the balance of hydrophobic interaction and electrostatic repulsion (Horne, 2020). Therefore, at a critical time, hydrophobic interactions prevail over electrostatic repulsion, and individual micelles start to interact with each other, forming aggregates that may flocculate. This further indicates that in order to create a system that avoids intensive CN flocculation, it is critical to determine the optimal salt concentrations. However, the phosphorylation degree may not be the single relevant factor for the instability of βκ-FP RCMS. Another possible factor could be increased hydrophobic interactions due to the enrichment of β-CN, the most hydrophobic CN (Fox & Brodkorb, 2008), facilitating enhanced self-association of the βκ-FP system. These factors may contribute to the excessive association within and between the CN micelles and further flocculation.

Additionally, the CaP stability of the βκ system was also influenced by the phosphorylation degree. Considerably increased proportions of micellar Ca^{2+} and P^{5+} of βκ-PP were observed (~48% and 37%, respectively) compared with βκ-FP (~7%), suggesting that a decreased CN-CaP interaction may sometimes limit the micelle excessive growth and hence increase micelle stability at certain conditions (in this case, when there are strong hydrophobic interactions). Moreover, similar to the four-CN systems, full dephosphorylation of the βκ-DP RCMS decreased the proportion of micellar CaP, resulting in the formation of CaP precipitates (~56% and ~40% of insoluble Ca^{2+} and P^{5+}, respectively) compared with βκ-PP (~16% of both insoluble Ca^{2+} and P^{5+}). These results combined indicate that decreasing the salts concentration and the phosphorylation degree to a desired level could help limit the excessive growth of micelles in the βκ system, thereby increasing CN and CaP stability.

3.4. Effect of phosphorylation degree on RCM size and structure

To initially estimate the size of the formed RCM, the average d_H values of the mildly centrifuged supernatants of the FP, PP, and DP RCMS were determined using DLS. As shown in Fig. S1, FP RCMS of all three systems had d_H values in the range of 139.0–156.3 nm, in accordance with CN micelle size reported in both skim milk and earlier RCMS studies (De Kruif & Huppertz, 2012; Fan et al., 2024). This value range appeared to be lower than those obtained for αβκ-DP and βκ-DP systems (173.6 ± 3.4 and 236.4 ± 8.5 nm, respectively). However, it is challenging to compare the particle sizes of RCM with varying degrees of phosphorylation based solely on d_H, owing to different particle distributions; the majority of DP CNs are in the serum fraction and likely to self-associate into complexes, whereas the major FP CNs form micelles together with CaP within the micellar fraction.

Therefore, to visualise changes in micellar structure in relation to phosphorylation degree, the mildly centrifuged supernatants of more

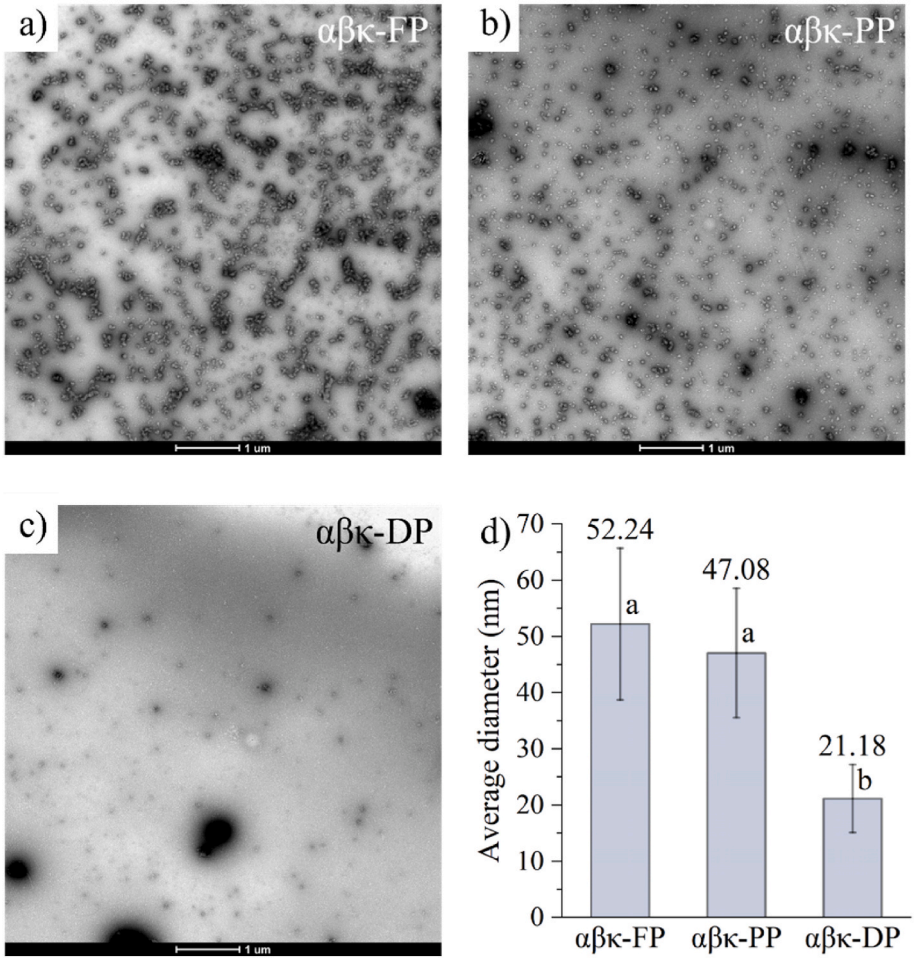

Fig. 5. Transmission electron microscope (TEM) images of the mildly centrifuged supernatant of αβκ-RCMS: **a)** FP, **b)** PP, and **c)** DP. Each image represents at least five observations. Scale bar = 1 μm. **d)** Comparison of average diameters of the RCM particles. Statistical analysis was performed using one-way ANOVA with Tukey's test.

stable αβκ RCMS were subjected to TEM. As shown in Fig. 5, the colour intensity observed in the images correlates with variations in the electron cloud density, where darker shades signify higher electron cloud densities (Reimer, 2013), corresponding to a higher density of aggregated CNs (Portnaya et al., 2006). The RCM of αβκ-FP showed a relatively homogenous distribution of micelles which seem to be spherical with an average diameter of 52.2 ± 13.5 nm. The smaller size compared with the DLS results could be attributed to micelle disruption and shrinkage resulting from i) temperature changes during sample storage and transportation (Marchin et al., 2007); ii) concentration changes during sample dilution (Hussain et al., 2011; Shukla et al., 2009); and iii) decreased hydration during the drying process (Huppertz et al., 2017; McMahon & McManus, 1998). Moreover, it is known that the visualisation of CN micelles by TEM is also challenged by artefacts introduced by the fixing and staining steps (Auty et al., 2005; McMahon et al., 1998).

Nevertheless, under the same sample preparation conditions, DP RCMS were prone to form smaller sporadic micelle structures with an average diameter of 21.2 ± 6.1 nm. The DP RCM was probably formed by the small remaining portion of PP CNs that survived dephosphorylation. The decreased particle size was presumably due to the reduced CN-CaP interaction, which was insufficient to facilitate CNs assembling into the normal micelle structures, along with size control by the relatively increased proportion of κ-CN. The major fully DP CNs, on the other hand, were self-associated in the serum fraction but disassociated at this dilution and thus were invisible by TEM. These results reaffirm that the lack of CN phosphorylation limits micelle formation.

3.5. Summary model of distribution and structural alterations of four-CN RCM due to CN dephosphorylation

To summarise, we speculated the model of distribution and structural alterations of four-CN RCM subjected to CN dephosphorylation, as illustrated in Fig. 6. In detail, compared with FP RCMS, i) the DP RCMS formed a similar proportion of insoluble CNs, whereas insoluble CaP increased remarkably; ii) the proportion of the micellar fraction of DP RCMS considerably decreased, with a small amount of CN and CCP remained; iii) the RCM structure formed by the remaining PP CNs within DP RCMS had decreased particle sizes; iv) the majority of DP CNs were in the serum and self-associated into complexes.

3.6. Effect of phosphorylation degree on RCMS acid-gelation ability

To study the pH stability relative to acid-gelation or precipitation of the RCMS in relation to the degree of phosphorylation, the rheology of the four-CN systems was investigated (Fig. 7a). For FP and PP RCMS, the G' was below 5 Pa at 60 min after GDL addition, indicating a very weak gel was formed at this condition. This is in accordance with the acid gelation study of skim milk without prior treatment (Horne, 2003; Li & Dalgleish, 2006), and the weak network was due to the highly hydrated interfaces and weak bonding between neighbouring particles (Dalgleish et al., 2012; Horne, 2020; Li et al., 2006).

However, the G' of DP RCMS at 60 min was considerably higher than those of FP and PP RCMS. From the correlation between pH and time, the onset of gelation or precipitation pH increases with decreasing phosphorylation degree (Fig. 7b), from an acid condition (~pH 5.0) to a more neutral condition (~pH 5.2 for PP and pH 5.5 for DP). This suggests a correlation with an increased isoelectric point (pI) after dephosphorylation (Sun et al., 2023). As the majority of CNs in DP RCMS remain in the serum fraction, the few micelles that form are unable to equilibrate and rearrange their structures like those in FP RCMS. This may have resulted in a higher elasticity at 60 min because of CN precipitation. Moreover, observation of the formed material with a continued pH drop for 3 h showed that the DP RCMS failed in gelation – the precipitates formed by DP RCMS remained unchanged after 1 h, whereas the gel formed by FP RCMS was firmer at 3 h than at 1 h (data not shown).

Combining these results, it is suggested that the DP CNs are unable to form CN micelle structures and thus fail in the sol-gel transition during acidification, instead precipitating into lumpy structures upon reaching the pI. Therefore, it is important to consider phosphorylation in yoghurt and cheese manufacturing of microbial CNs, and their acid- and rennet-coagulation behaviour in relation to the degree of phosphorylation warrants further investigation when compared to FP RCMS and skim

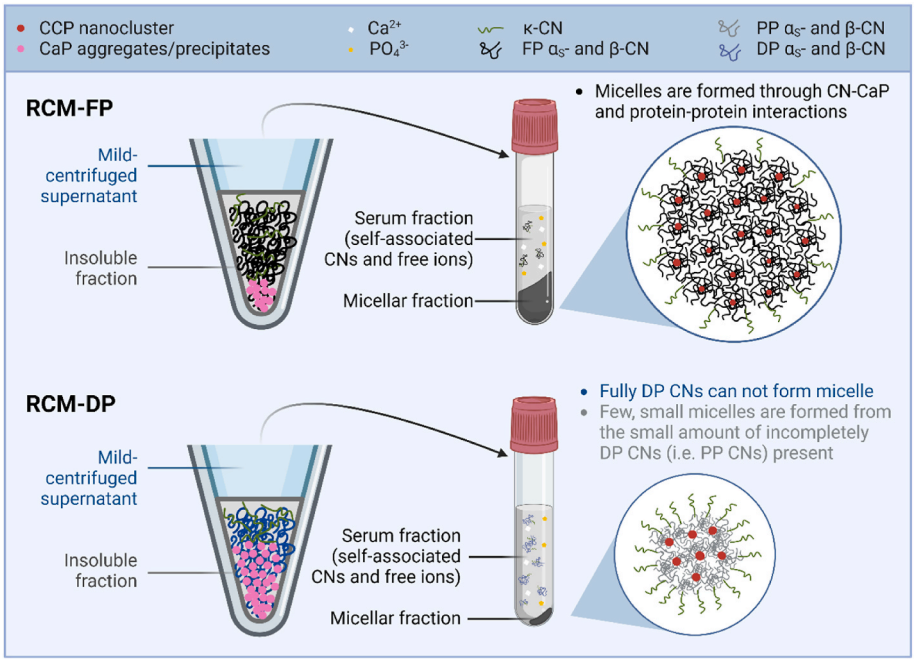

Fig. 6. Illustration of RCMS models of four-CN systems with FP and DP CNs showing the variation in content across fractions and the micelle structure. The increased CCP nanocluster size of DP RCM compared to FP was speculated based on the work of Antuma et al. (2023), which assumed that all CNs interacted with CaP in SAXS modelling. Created with BioRender.com. Not to scale.

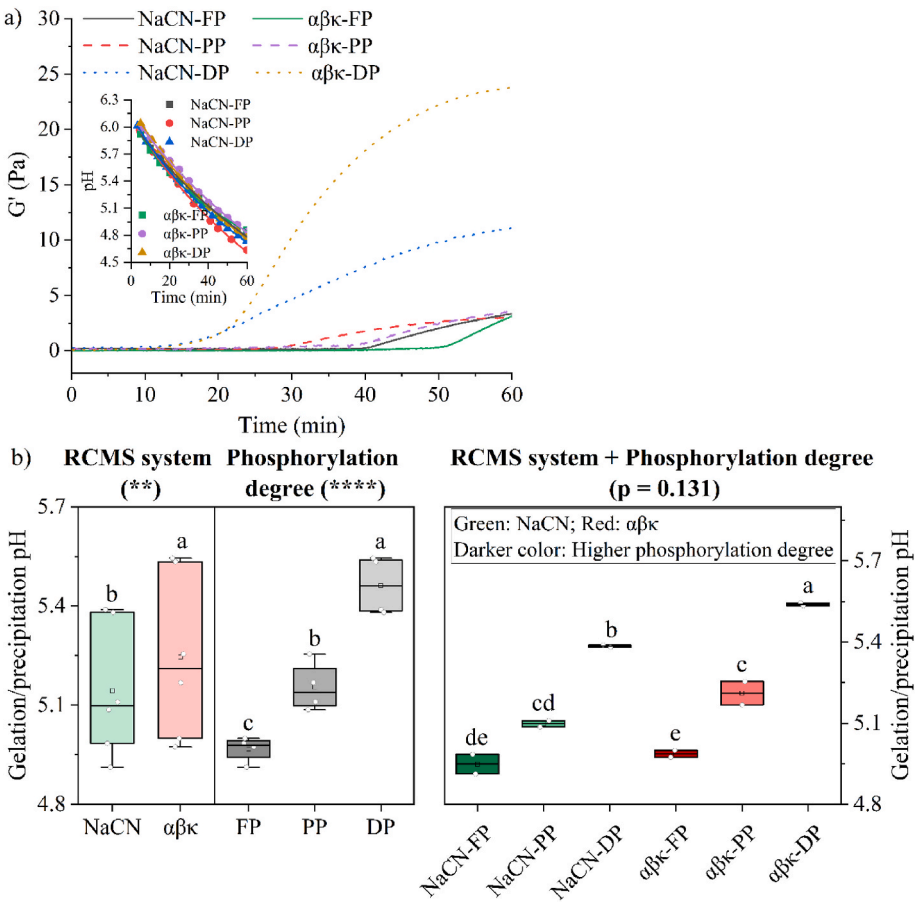

Fig. 7. a) Changes in G′ and pH (inset figure) over time with the addition of GDL. **b)** Comparison of gelation or precipitation pH across two RCMS systems ($p = 0.002$, $n = 6$), three phosphorylation degrees ($p < 0.0001$, $n = 4$), and the interaction effects of RCMS system and phosphorylation degree on gelation or precipitation pH ($p = 0.131$, $n = 2$). Statistical analysis was performed using two-way ANOVA with Tukey's test.

milk.

3.7. Implication for future dairy production using microbial CNs

Moving forward, since the general stability, calcium-binding ability, and acid-gelation ability of the DP RCMS were considerably lower than those of FP RCMS, additional *in vitro* phosphorylation processes may be necessary to utilise microbial CNs in future dairy products. Moreover, the best functionalities of the RCMS in this study were obtained using the four CNs with native phosphorylation degrees. However, using kinases to achieve 'ultrahigh' phosphorylation degrees in microbial CNs may be possible, and it would be interesting to explore their RCMS stability and functionality as a potentially superior functional dairy alternative product compared to those currently available.

Additionally, further investigations are required to facilitate a better understanding of the functionalities of these microbial CNs in many aspects: i) investigating functional properties such as acid- and rennet-coagulation, digestibility, emulsifying properties, water-holding capacity, and drug delivery and release; ii) studying the RCM structure and functionality when supplied with other ingredients, such as whey proteins, fat, and lactose; iii) investigating the RCMS stability and corresponding byproducts during various processing treatments, such as heating, cooling, and high pressures; iv) exploring the additional PTMs (e.g. glycosylation) and impact of disulfide bonds and studying the effect of these modifications especially if they differ from that of bovine CNs; v) investigating the feasibility of recombining bovine genes with known functional properties, such as β-CN A2 variants, into microbials and assessing their impact on functionality of the products.

4. Conclusions

In this study, the effect of phosphorylation degree of purified bovine CNs on micelle reassembly and stability under neutral and acidic conditions was studied using FP, PP, and DP CNs. To the best of our knowledge, this study is the first to evaluate the detailed composition and stability of RCMS by separating the insoluble components from micellar and serum fractions. We confirmed the essential role of CN phosphorylation in micelle reassembly, and observed a positive correlation between the degree of phosphorylation and the proportion of micellar fraction, as well as RCMS stability. The fully DP CNs were unable to stabilise CaP and form a CN micelle structure, but were self-associated in the serum fraction. The acid-gelation ability was found to be influenced by phosphorylation, with fully DP CNs failing in gelation but rather precipitating at a higher pH (5.5) than the gelation pH of FP CNs (5.0) or PP CNs (5.2). In addition, the RCMS containing only β/κ-CN at their native full phosphorylation degree was unstable at the salt concentrations applied, with more than half of the CNs self-associating to flocculate. These results highlighted the potential functionality of PP CNs while also underscoring the necessity for additional *in vitro* phosphorylation of microbial CNs, as FP CNs provided optimal properties such as calcium-binding and gelation. This process is crucial for ensuring their suitability in dairy manufacturing, particularly given the lower phosphorylation levels of CNs produced by precision fermentation.

CRediT authorship contribution statement

Jing Che: Writing – review & editing, Writing – original draft,

Visualization, Methodology, Investigation, Formal analysis, Data curation, Conceptualization. **Zekun Fan:** Writing – review & editing, Writing – original draft, Methodology. **Etske Bijl:** Writing – review & editing, Supervision. **Julia Prangchat Stub Thomsen:** Writing – review & editing. **Ivan Mijakovic:** Writing – review & editing. **Kasper Hettinga:** Writing – review & editing, Supervision. **Nina Aagaard Poulsen:** Writing – review & editing, Supervision, Conceptualization. **Lotte Bach Larsen:** Writing – review & editing, Supervision, Project administration, Funding acquisition, Conceptualization.

Declaration of competing interest

The authors declare that they have no known competing financial interests or personal relationships that could have appeared to influence the work reported in this paper.

Data availability

Data will be made available on request.

Acknowledgements

This work was supported by the Novo Nordisk Foundation, Denmark (NNF) via the DECIPHER project (grant number NNF21OC0071334), the Danish Dairy Research Foundation, Denmark (DDRF) via the CleanMilk project, Aarhus University, Denmark via the Graduate School of Technical Sciences (GSTS), and by China Scholarship Council, China (CSC). The work is also part of the 'Animal-free milk proteins' project (project number NWA.1292.19.302) of the NWA research program 'Research along Routes by Consortia (ORC)', which is funded by the Dutch Research Council, the Netherlands (NWO).

Jens Berndtsson was acknowledged for imaging TEM figures. Wanxiang Guo was acknowledged for language editing of the manuscript. Fællesfonden and William Demant Fonden, Denmark were acknowledged for supporting the research stay of J. Che in the Netherlands. We acknowledge the funding from the Swedish Research Council, Sweden Vetenskapsrådet (grant number 391 2020-03176) and the Novo Nordisk Foundation (grant number NNF20CC0035580) to I. Mijakovic.

Appendix A. Supplementary data

Supplementary data to this article can be found online at https://doi.org/10.1016/j.foodhyd.2024.110615.

References

Antuma, L. J., Steiner, I., Garamus, V. M., Boom, R. M., & Keppler, J. K. (2023). Engineering artificial casein micelles for future food: Is casein phosphorylation necessary? *Food Research International, 173*(1), Article 113315.

Auty, M. A., O'Kennedy, B. T., Allan-Wojtas, P., & Mulvihill, D. M. (2005). The application of microscopy and rheology to study the effect of milk salt concentration on the structure of acidified micellar casein systems. *Food Hydrocolloids, 19*(1), 101–109.

Bijl, E., Holland, J. W., & Boland, M. (2020). Posttranslational modifications of caseins. In *Milk proteins* (pp. 173–211). Academic Press.

Bijl, E., Huppertz, T., van Valenberg, H., & Holt, C. (2019). A quantitative model of the bovine casein micelle: Ion equilibria and calcium phosphate sequestration by individual caseins in bovine milk. *European Biophysics Journal, 48*(1), 45–59.

Bijl, E., van Valenberg, H. J., Huppertz, T., & van Hooijdonk, A. C. (2013). Protein, casein, and micellar salts in milk: Current content and historical perspectives. *Journal of Dairy Science, 96*(9), 5455–5464.

Booth, D. S., Avila-Sakar, A., & Cheng, Y. (2011). Visualizing proteins and macromolecular complexes by negative stain EM: From grid preparation to image acquisition. *Journal of Visualized Experiments: JoVE*, (58), Article e3227.

Dalgleish, D. G., & Corredig, M. (2012). The structure of the casein micelle of milk and its changes during processing. *Annual Review of Food Science and Technology, 3*, 449–467.

De Kruif, C. G., & Holt, C. (2003). Casein micelle structure, functions and interactions. In *Advanced dairy chemistry—1 proteins: Part a/part b* (pp. 233–276). Boston, MA: Springer US.

De Kruif, C. G., & Huppertz, T. (2012). Casein micelles: Size distribution in milks from individual cows. *Journal of Agricultural and Food Chemistry, 60*(18), 4649–4655.

De Kruif, C. G., Huppertz, T., Urban, V. S., & Petukhov, A. V. (2012). Casein micelles and their internal structure. *Advances in Colloid and Interface Science, 171–172*, 36–52.

Fan, Z., Fehér, B., Hettinga, K., Voets, I. K., & Bijl, E. (2024). Effect of temperature, pH and calcium phosphate concentration on the properties of reassembled casein micelles. *Food Hydrocolloids, 149*.

Fox, P. F., & Brodkorb, A. (2008). The casein micelle: Historical aspects, current concepts and significance. *International Dairy Journal, 18*(7), 677–684.

Hansson, L., Bergström, S., Hernell, O., Lönnerdal, B., Nilsson, A. K., & Strömqvist, M. (1993). Expression of human milk beta-casein in Escherichia coli: Comparison of recombinant protein with native isoforms. *Protein Expression and Purification, 4*(5), 373–381.

Hettinga, K., & Bijl, E. (2022). Can recombinant milk proteins replace those produced by animals? *Current Opinion in Biotechnology, 75*, Article 102690.

Holt, C. (1992). Structure and stability of bovine casein micelles. *Advances in Protein Chemistry, 43*, 63–151.

Holt, C., Carver, J. A., Ecroyd, H., & Thorn, D. C. (2013). Invited review: Caseins and the casein micelle: Their biological functions, structures, and behavior in foods. *Journal of Dairy Science, 96*(10), 6127–6146.

Horne, D. S. (2003). Casein micelles as hard spheres: Limitations of the model in acidified gel formation. *Colloids Surf A Physicochem Eng Aspects, 213*(2–3), 255–263.

Horne, D. S. (2020). Casein micelle structure and stability. In *Milk proteins* (pp. 213–250). Academic Press.

Huppertz, T., Gazi, I., Luyten, H., Nieuwenhuijse, H., Alting, A., & Schokker, E. (2017). Hydration of casein micelles and caseinates: Implications for casein micelle structure. *International Dairy Journal, 74*, 1–11.

Hussain, R., Gaiani, C., Aberkane, L., Ghanbaja, J., & Scher, J. (2011). Multiscale characterization of casein micelles under NaCl range conditions. *Food Biophysics, 6*(4), 503–511.

Li, J., & Dalgleish, D. G. (2006). Controlled proteolysis and the properties of milk gels. *Journal of Agricultural and Food Chemistry, 54*(13), 4687–4695.

Li-Chan, E., & Nakai, S. (1989). Enzymic dephosphorylation of bovine casein to improve acid clotting properties and digestibility for infant formula. *Journal of Dairy Research, 56*(3), 381–390.

Marchin, S., Putaux, J. L., Pignon, F., & Léonil, J. (2007). Effects of the environmental factors on the casein micelle structure studied by cryo transmission electron microscopy and small-angle x-ray scattering/ultrasmall-angle x-ray scattering. *The Journal of Chemical Physics, 126*(4), Article 045101.

McMahon, D. J., & McManus, W. R. (1998). Rethinking casein micelle structure using electron microscopy. *Journal of Dairy Science, 81*(11), 2985–2993.

Patel, S. G., Patel, M. D., Patel, A. J., Chougule, M. B., & Choudhury, H. (2018). Solid lipid nanoparticles for targeted brain drug delivery. In *Nanotechnology-based targeted drug delivery systems for brain tumors* (pp. 191–244). Academic Press.

Portnaya, I., Cogan, U., Livney, Y. D., Ramon, O., Shimoni, K., Rosenberg, M., & Danino, D. (2006). Micellization of bovine beta-casein studied by isothermal titration microcalorimetry and cryogenic transmission electron microscopy. *Journal of Agricultural and Food Chemistry, 54*(15), 5555–5561.

Poulsen, N. A., Jensen, H. B., & Larsen, L. B. (2016). Factors influencing degree of glycosylation and phosphorylation of caseins in individual cow milk samples. *Journal of Dairy Science, 99*(5), 3325–3333.

Reimer, L. (2013). *Transmission electron microscopy: Physics of image formation and microanalysis* (Vol. 36). Springer.

Schmidt, D. G., Koops, J., & Westerbeek, D. (1977). Properties of artificial casein micelles. 1. Preparation, size distribution and composition. *Netherlands Milk and Dairy Journal, 31*, 328–341.

Schmidt, D. G., & Poll, J. K. (1989). Properties of artificial casein micelles. 4. Influence of dephosphorylation and phosphorylation of the casein. *Netherlands Milk and Dairy Journal, 43*(1), 53–62.

Sheng, B., Nielsen, S. D., Glantz, M., Paulsson, M., Poulsen, N. A., & Larsen, L. B. (2022). Effects of genetic variants and sialylation on in vitro digestibility of purified kappa-casein. *Journal of Dairy Science, 105*(4), 2803–2814.

Shukla, A., Narayanan, T., & Zanchi, D. (2009). Structure of casein micelles and their complexation with tannins. *Soft Matter, 5*(15), 2884–2888.

Sun, X., Anema, S. G., & Gerrard, J. A. (2023). The effect of dephosphorylation on the properties of αS1-casein enriched protein. *International Dairy Journal, 146*.

Tubiello, F. N., Salvatore, M., Rossi, S., Ferrara, A., Fitton, N., & Smith, P. (2013). The FAOSTAT database of greenhouse gas emissions from agriculture. *Environmental Research Letters, 8*(1), Article 015009.

Wang, X., & Zhao, Z. (2022). Acid-induced gelation of milk: Formation mechanism, gel characterization, and influence of different techniques. In *Current issues and advances in the dairy industry*. IntechOpen.